Proceedings of the 1998 IEEE
International Conference on Robotics & Automation
Leuven, Belgium • May 1998

DLR's multisensory articulated Hand
Part II: The Parallel Torque/Position Control System

H. Liu P. Meusel J. Butterfass G. Hirzinger

DLR
German Aerospace Center
Institute of Robotics and System Dynamics, 82230 Wessling
e-mail: Hong.Liu@dlr.de

Abstract

This paper gives a brief description of feedback control systems engaged in DLR's recently developed multi-sensory 4 finger robot hand. The work is concentrated on constructing the dynamic model and the control strategy for one joint of the fingers. One goal is to make the hand follow a dataglove for fine manipulation tasks. Our proposed strategy for this task is parallel torque/position control; sliding mode control is realized for the robust trajectory tracking in free space; while impedance control is provided for compliance control in the constrained environment; and an easily-designed parallel observer is used for the switch between these two control modes during the transition from or to contact motion. Some experimental results show the effectiveness of proposed strategy for the pure position control, torque control, and the transition control.

1. Introduction

The DLR's multisensory articulated hand[1], as shown in Fig. 1, is a four fingered hand with in total twelve degrees of freedom. It has three fingers and an opposing thumb. The actuation system is uniformly based on Artificial Muscles®[1], a tiny linear electromechanical actuator integrating DLR's planetary roller screw-drive[2] with small brushless DC motor(BLDC), which are integrated in the hand's palm or in the fingers directly. Force transmission in the fingers is realized by special tendons made of highly molecular polyethylene. To achieve high degree of modularity, all four fingers are identical, and each has three active DOFs and integrates 28 sensors. The motions of middle phalanx and distal phalanx are not individually controllable; they are connected by means of tendons in such a way as to display motions similar to those of human fingers during grasping and are actuated only by one artificial muscle. The proximal joint has 2 degrees of freedom; one is for curling motion and another is for abduction/adduction motion.

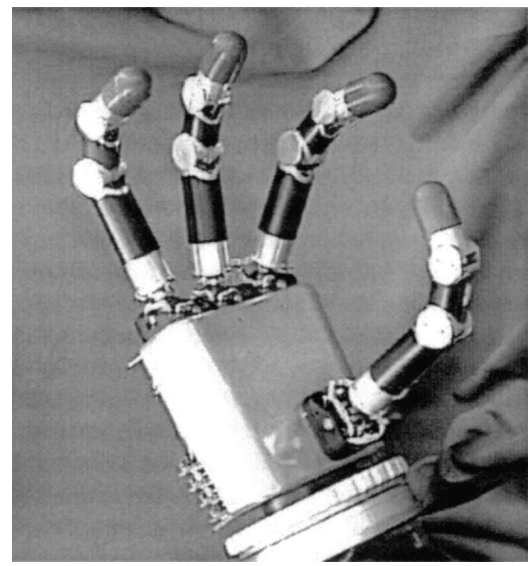

Fig. 1. The DLR's Multisensory Hand

There are two different position sensors for each active degree of freedom; one is a tracking converter for measuring the motor position on the basis of Hall sensors and another is the actual joint position sensor based on a one-dimensional PSD (Position Sensing Device), which is illuminated by an infrared LED via an etched spiral-type measurement slot. The effective combination between these two kind of sensors plays a key role in the joint position control in dealing with tendon hysteresis. Also, at each joint there is a torque sensor based on strain-gauges for accurate torque control. A more detailed description is given in Part I.

Our first approach was to make the hand to follow the desired states (positions, speeds, accelerations, and torques) commanded from higher levels, e.g., dataglove. This requires accurate tracking in free space, compliance in the constrained environment, and smooth transition between these two operational modes.The tracking control problem is to design a control scheme which generates the appropriate control signal so as to ensure that the joint angle follows any specified reference trajectory as closely

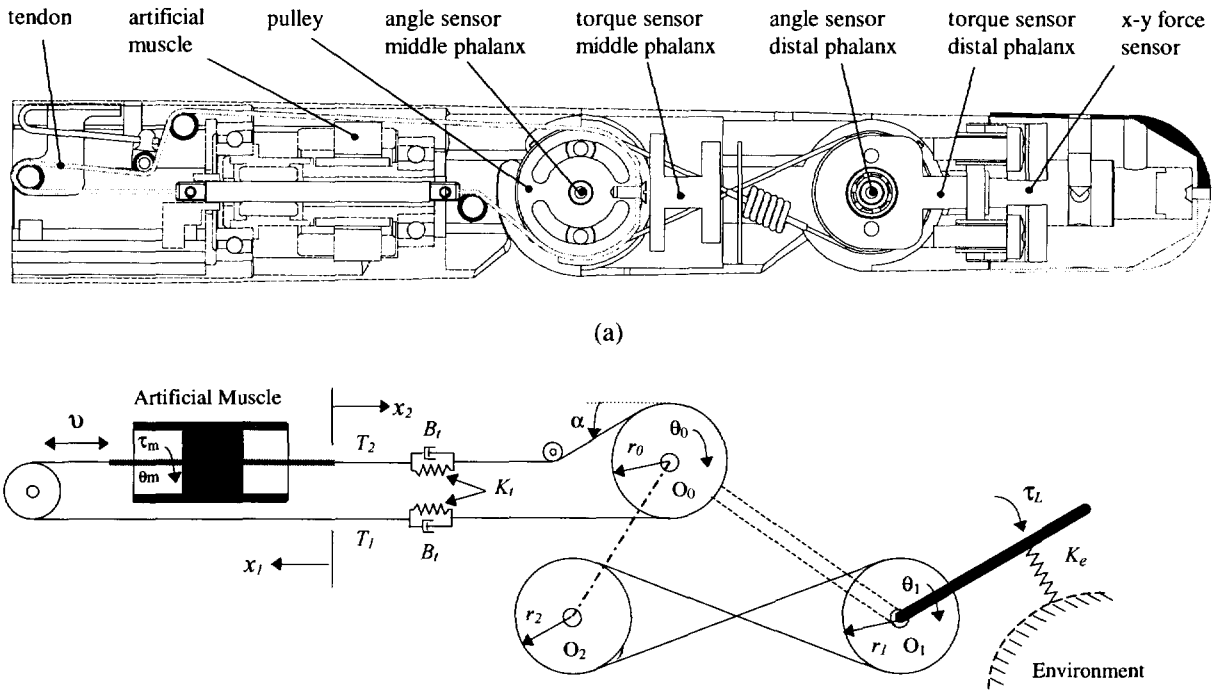

Fig.2 The Finger Mechanical Construction(a) and Its Schematic Diagram (b)

as possible. Compliance control is needed for fine manipulation and also for the protection of the hand itself. Transition control, called also impact control, is essentially the problem of making the energy conversion more effective and smooth. The well-known approaches to transition control include impedance control[3] and explicit force control[4]. Although the control schemes show good performance, this performance is achieved under fairly restrictive conditions. Common to the approaches is the requirement that the operating environment as well as the environmental interaction have to be very accurately modeled. This fact restricts their use in realistic operating environments. In this paper we propose a parallel torque/position control strategy for the pre-described task. The robust trajectory tracking in free space is implemented by sliding mode control; the compliant motion in the constrained environment is realized by using impedance control; and a parallel observer based on contact torques and system states has been built to determine the switch between these two kind of controllers for the transition control from or to contact motion.

2. Dynamic Model of a Joint

The actuation and transmission system of the third link of the DLR four-fingered hand is shown in Fig. 2(a). The main components of the single-joint model are : a) the BLDC-based artificial muscle; b) the tendon pulley power transmission system; and c) the joint itself. The artificial muscle is a linear actuator which translates the motor's rotation into axial movements based on DLR's planetary roller screw drive[2]. The tendon as a structure is represented by parallel spring and damping elements(K_{st}, B_{st}), which permit the structural oscillations between the actuator and load. A schematic diagram of the system is shown in Fig. 2(b). T_1 and T_2 represent the tension in the tendon at the appropriate points while T_{10} and T_{20} represent the corresponding pretensions. τ_L represents the external torque which results from the contact between the finger and its environment, and K_e is the environment stiffness. The system also exhibits a hysteresis effect due to the combination of Coulomb friction and tendon compliance. Fig.7(a) shows the experimental hysteresis measurements. Hystereses windup and winddown only occur during the initial startup, or result from direction changes. One may then write down the following equations describing the dynamics of the finger unit:

$$r_0 = r_2 = K_r r_1 \tag{1}$$

$$\theta_1(t) = n\theta_m(t), \theta_1(t) = K_r\theta_o(t) \tag{2}$$

$$T_1 = K_t(x_1(t) - r_0\theta_0(t)) + B_t(\dot{x}_1(t) - r_o\dot{\theta}_0(t)) + T_{10} \tag{3}$$

$$T_2 = K_t(x_2(t) - r_0\theta_0(t)) + B_t(\dot{x}_2(t) - r_o\dot{\theta}_0(t)) + T_{20} \tag{4}$$

$$\tau_m = K_I I_m \tag{5}$$

$$J_m\ddot{\theta}_m(t) + B_m\dot{\theta}_m(t) + T_f + T_g + n\tau_L = \tau_m \tag{6}$$

$$\tau_L + K_s\left(\theta_1(t) - x_1(t)/r_1\right) = 0 \tag{7}$$

where the remaining parameters are defined in Tabel 1.

3. Sliding Mode Position Control of a Joint

The theory and properties of sliding mode control[5] are well known in the automatic control field. The important features of the sliding mode controller which make it attractive for application in the power electronics area are a) high accuracy, b) fast dynamic response, c) good stability, d) simplicity of design and implementation, and, above all, e) robustness. Robustness, or low sensitivity to deviations in system parameters and external disturbances , is a very important index of the controller in industrial applications. Melchiorri[6] used the sliding mode technique for the position control of the University of Bologna (UB) hand, however he did not deal with the trajectory tracking problems. The goal of the research activity presented in this paper is to experimentally verify the feasibility of a sliding mode controller for the position tracking control of the third joint.

To design the position controller with sliding mode properties, the dynamic equation (6) is rewritten in terms of state space:

$$x_1 = \theta_m,\ x_2 = \dot{x}_1,\ x_3 = \dot{x}_2$$

$$\begin{bmatrix}\dot{x}_1\\ \dot{x}_2\\ \dot{x}_3\end{bmatrix} = \begin{bmatrix}0 & 1 & 0\\ 0 & 0 & 1\\ 0 & -\frac{B_m R_m}{J_m L_m} & -\left(\frac{B_m}{J_m}+\frac{R_m}{L_m}\right)\end{bmatrix}\begin{bmatrix}x_1\\ x_2\\ x_3\end{bmatrix} + \begin{bmatrix}0\\ 0\\ \frac{K_I R_m}{J_m L_m}\end{bmatrix} I_m + \begin{bmatrix}0\\ 0\\ -\frac{R_m}{J_m L_m}\end{bmatrix}(T_f + T_g + n\tau_L) \tag{8}$$

Equation (8) is in the form of

$$\dot{X} = AX + bu + Dn \tag{9}$$

where the control u takes the form of the link current I_m, and the disturbance input n is the load torque $n\tau_L$, friction T_f, and gravitation T_g.

Let $R(t) = [\theta_d\ \dot{\theta}_d\ \ddot{\theta}_d]^T$ be a reference track vector, i.e. a vector containing the desired tracks of motor position, speed and acceleration, $X(t)$ is the system state vector. Let the error $E(t)$ be defined as follows:

$$E(t) = R(t) - X(t) \tag{10}$$

The switching surface s here is chosen as

$$s(t) = C \cdot E(t),\ C = [c_1\ c_2\ c_3],\ E(t) = [e_1\ e_2\ e_3]^T,$$

where C is a vector of weighting factors and c_3=1. The switching surface is defined as $s(t) = 0$.

The control law of the sliding mode control is as follows

$$u = \psi_1 e_1 + \psi_2 e_2 + d\,\mathrm{sgn}(s) \tag{11}$$

where ψ_1 and ψ_2 are feedback gains of each state variable and d is the input gain for compensating disturbances. The term $d\,\mathrm{sgn}(s)$ is a steady-state dither component that is used to remove the steady-state error. Note that parameters ψ_1, ψ_2 and d in equation (11) allow changes in the individual terms, whereas d allows changes common to all the terms. Parameters ψ_1 and ψ_2 are not fixed , but change discretely to maintain the system on the switching surface.

3.1 Conditions of existence

The existence conditions of sliding mode require that the state trajectories be always directed towards the sliding surface s. This is given in mathematical form as

$$\lim_{s\to o} s(t)\cdot\frac{ds(t)}{dt} \le 0 \tag{12}$$

From equations (8), (10), and (11),

$$\begin{aligned} s\dot{s} &= (c_1\dot{e}_1 + c_2\dot{e}_2 + \dot{e}_3)s \\ &\approx \left(-c_1c_2 + c_1\left(\frac{B_m}{J_m}+\frac{K_I}{J_m}\right) - \frac{K_I R_m}{J_m L_m}\psi_1\right)e_1 s \\ &+ \left(-c_2\left(c_2 - \frac{B_m}{J_m} - \frac{K_I}{J_m}\right) + c_1 - \frac{B_m R_m}{J_m L_m} - \frac{K_I R_m}{J_m L_m}\psi_2\right)e_2 s \\ &+ \left(\frac{R_m}{J_m L_m}\left(T_f + T_g + n\tau_L\right) + \dot{r}_3 + \left(\frac{B_m}{J_m}+\frac{R_m}{L_m}\right)r_3 + \frac{B_m R_m}{J_m L_m}r_2\right)s \\ &- \frac{K_I R_m}{J_m L_m} d\,\mathrm{sgn}(s)s \end{aligned}$$

The existence condition of sliding mode given in (12) can be satisfied if

$$\begin{aligned} d > &\frac{1}{K_I}\left(T_f + T_g + \tau_L\right) \\ &+ \frac{J_m L_m}{K_I R_m}\left(\frac{B_m R_m}{J_m L_m}r_2 + \dot{r}_3 + \left(\frac{B_m}{J_m}+\frac{R_m}{L_m}\right)r_3\right) \end{aligned} \tag{13}$$

$$\psi_1 = \begin{cases} \alpha_1 & if\ e_1 s > 0 \\ \beta_1 & if\ e_1 s > 0 \end{cases} \tag{14}$$

$$\psi_2 = \begin{cases} \alpha_2 & if\ e_2 s > 0 \\ \beta_2 & if\ e_2 s > 0 \end{cases} \tag{15}$$

where,

$$\alpha_1 = \max_t \left\{ \frac{J_m L_m}{K_I R_m} \left(-c_1 c_2 + c_1 \left(\frac{B_m}{J_m} + \frac{K_I}{J_m} \right) \right) \right\}$$

$$\beta_1 = \min_t \left\{ \frac{J_m L_m}{K_I R_m} \left(-c_1 c_2 + c_1 \left(\frac{B_m}{J_m} + \frac{K_I}{J_m} \right) \right) \right\}$$

$$\alpha_2 = \max_t \left\{ \frac{J_m L_m}{K_I R_m} \left(c_1 - c_2 \left(c_2 - \frac{B_m}{J_m} - \frac{K_I}{J_m} \right) - \frac{B_m R_m}{J_m L_m} \right) \right\}$$

$$\beta_2 = \min_t \left\{ \frac{J_m L_m}{K_I R_m} \left(c_1 - c_2 \left(c_2 - \frac{B_m}{J_m} - \frac{K_I}{J_m} \right) - \frac{B_m R_m}{J_m L_m} \right) \right\}$$

3.2 Conditions of stability

In order to make the motion in the sliding regime stable, the coefficient c_i needed for the design of a desired sliding mode cannot be chosen freely. Considering the motion on the sliding surface $s=0$, the characteristic equation is

$$\ddot{e}_1 + c_2 \dot{e}_1 + c_1 = 0 \tag{16}$$

Since we do not want any overshoot, our choice of c_1 and c_2 must satisfy the condition:

$$c_2 \geq 2\sqrt{c_1}\ ;\ c_1, c_2 \geq 0 \tag{17}$$

3.3 Conditions of hitting

In order to guarantee that the system hits the sliding surface s from any initial states, the following condition should be satisfied [5]

$$c_2 < \frac{B_m}{J_m} + \frac{R_m}{L_m} \tag{18}$$

Equations (13), (14), (15), (17), and (18) together specify the bounds on the controller parameters for operation of the position tracking control system in sliding mode. From these equations it is clear that exact knowledge of system parameters is not necessarily needed for designing the sliding mode controller. It is sufficient to know the bounds on the system parameters for the design of the above controller.

3.4 Practical implementation of the SLM

The sliding mode controller is constructed using the position error, speed error, and acceleration error. The practical implementation is shown in Fig.3. The reference trajectory is produced through a fifth-order polynomial interpolation when the desired position and speed are given[6].

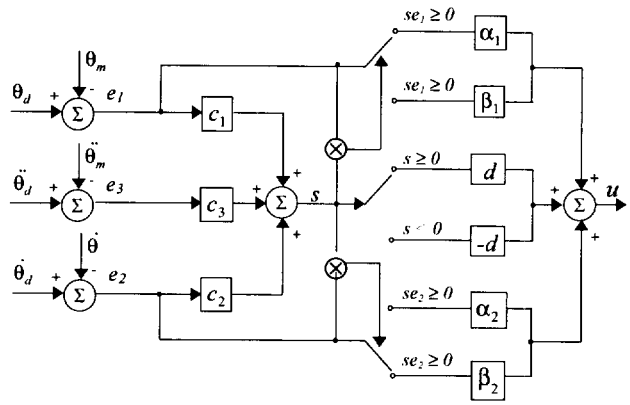

Fig.3 Block diagram of SLM position control of a joint

4. Impedance Joint Torque Control

Let J_d, B_d, K_d be the desired target impedance parameters of the robot finger; impedance control specifies this desired impedance relationship as a generalization of the second order dynamics of a damped spring:

$$J_d \ddot{\theta}_e + B_d \dot{\theta}_e + K_d \theta_e = \tau_{ext} \tag{19}$$

where $\theta_e = \theta_d - \theta_m$ is the position error, while θ_d, θ_m, and τ_{ext} are the desired position, actual joint position, and the actual reaction force which the environment exerts on the robot finger, respectively. In order to keep the target impedance, one can deduce the following motor output torque by introducing (19) into (6):

$$\tau_m = J_m \left\{ \ddot{\theta}_d + J_d^{-1} \left[B_d (\dot{\theta}_d - \dot{\theta}_m) + K_d (\theta_d - \theta_m) - \tau_{ext} \right] \right\} + B_m \dot{\theta}_m + T_f + T_g + n\tau_L \tag{20}$$

This means that, with precise knowledge of finger dynamics and accurate sensors, one can achieve a perfect feedback linearization for driving torque calculation, and

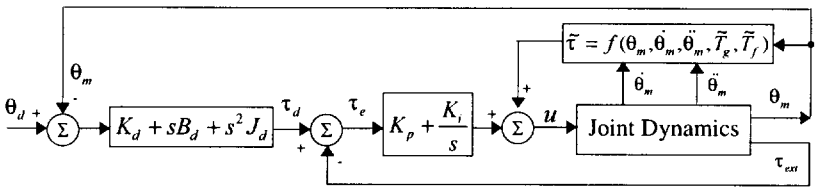

Fig. 4. Block Diagram of Impedance Torque Control

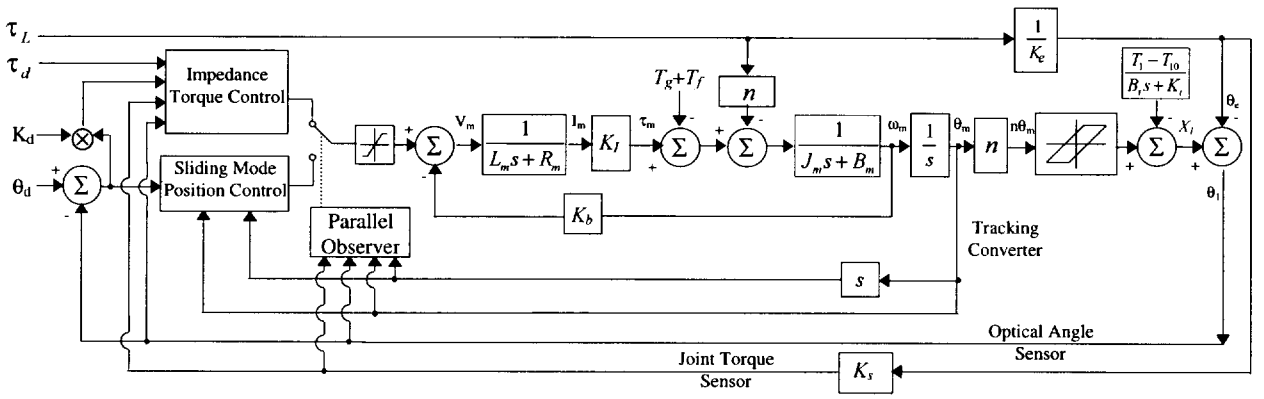

Fig. 5. Block diagram of the parallel torque/position control system

TABLE 1 : PARAMETERS OF ARTIFICIAL MUSCLE(AM20) AND TRANSMISSION SYSTEM

K_I = 9.0x10^{-3} *Nm/A*	torque constant	t_E = 0.14 *ms*	electrical time constant
J_m = 1.62x10^{-7} *Kg.m^2*	total inertia	t_M = 4.17 *ms*	mechanical time constant
B_m = 1.11x10^{-4} *Nm/rad/s*	damping coefficient	K_s = 2.73x10^1 *Nm/rad*	stiffness of sensing joint
K_b = 2.0x10^{-2} *V/rad/s*	back EMF constant	T_1, T_2	tendon tension
L_m = 1000.0 μ*H*	armature inductance	K_t = 2.86x10^4 *N/m*	tendon stiffness constant
R_m = 7.0 Ω	ave. Terminal resistance	B_t = 5.6x10^{-4} *Nm/rad/s*	tendon damping constant
n = 1/323	reducer ratio	K_r = 1.05	pulley radii reducer ratio
I_m	motor link current	T_g	gravitational force
τ_m	motor output torque	T_f	frictional force

the finger will show up the desired impedance parameters -- J_d, B_d, K_d to the environment. However, in reality, the finger dynamics are not known precisely, tendon transmission brings some hysteresis, and the accuracy of the position and torque sensors are always affected by some noises. This means, practically, that it would be very difficult to realize a perfect linearization, and hence the desired impedance parameters can not be achieved. Alternatively, in order to keep the equality (19) as equal as possible, we can also introduce an explicit force control scheme, i.e. , let

$$\tau_d = J_d(\ddot{\theta}_d - \ddot{\theta}_m) + B_d(\dot{\theta}_d - \dot{\theta}_m) + K_d(\theta_d - \theta_m) \qquad (21)$$

where τ_d is the desired torque. let τ_e be the error function:

$$\tau_e = \tau_d - \tau_{ext} \qquad (22)$$

Now we can introduce a simple PI control scheme with τ_e as input. If the τ_e converges to zero, the actual impedance parameters will converge to the desired values automatically. With the addition of the control signal from PI and estimated finger dynamics, we can build an impedance controller shown in Fig.4. However the desired trajectory is not specified as a fixed function of time. Instead, it is a varying information from a high level, e.g. from a dataglove. In steady state, all measured and desired velocity and acceleration values are zero. This induces that the value of the steady state torque is the stiffness multiplied by the steady state deformation $(\theta_d - \theta_m)$, and the joint behaves like a programmable spring.

5. Parallel Torque/Position Control Strategy

Motions in free space and constrained environment belong to different operational modes with a qualitative change in the system model. In the previous section the sliding mode position control and impedance torque control have been introduced for these two motion modes. Some experimental results will be discussed in the next section. Pure position control systems will follow the commanded position trajectory while rejecting external forces which are considered as disturbances. Force control is introduced for the motion control in the constrained environment by tracking a dynamic relation between the

active force and impedance. During the transition phase a large amount of kinematical energy need to be dissipated within a very short time. There exists a key problem of how to deal with the transition from free space to constrained environment or vice versa.

In this paper we propose a parallel torque/position control strategy for the transition phase, which is shown in Fig. 5. The strategy attempts to combine simplicity and robustness of the impedance control and sliding mode control with the ability of controlling both torque and position. The kernel of the strategy is the design of a parallel observer which determines which control mode should be active. The inputs to the observer are active torques, actual system states, and desired system states. Fig. 6 shows the block diagram of the parallel observer, where τ_{th} is the initial contact detecting torque and *i, i-1* represent the current and previous events. The mode switching to contact motion is only determined by contact torque, while the recovering from contact motion to free motion is not only determined by τ_{th} but also dependent on whether the reference position changes. There is always one control mode active. The control signal exhibits a discontinuity only when the control mode has been changed. In order to make the transition phase as smooth as possible, a first-order low-pass filter is used for the control signal variations.

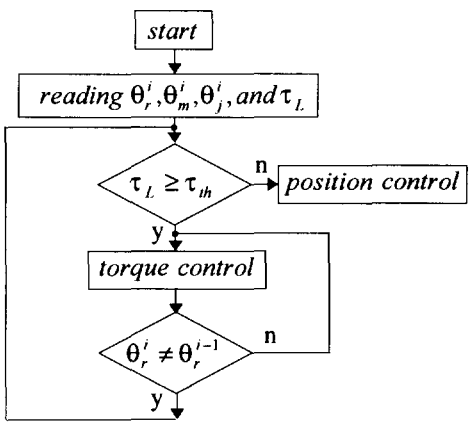

Fig. 6 Block diagram of parallel observer

6. Experimental Results

To verify the proposed control approach, a DSP(Digital Signal Processor)-based real-time control system has been built. The kernel of the system is a commercially available processor board with a TMS320C40. Some characteristics of this board are: 50 MHz clock(40 ns cycle time), floating point arithmetic unit, 768 Kbyte of fast static memory; and there are several I/O boards such as ADC, DAC, PIO which are installed in a separate box . All software development is done on the separate box which connects to a SUN workstation via ether net. The box takes care of the user interface, while most real-time computations and data I/O needed for the hand control are performed by several DSP boards.

Fig. 7(b) shows the sliding mode position control in free space, where there are two position sensors denoted by '1' and '2' which represent the motor position and actual joint position, respectively. Due to the hysteresis of tendon transmission and the slippage of the artificial muscle, there is always about 2° backlash between '1' and '2'. Our goal is to enable the motor to follow a desired trajectory as closely as possible and at the same time to achieve an accurate end-point position. Therefore, a dynamic variable reference trajectory is built, which changes according to the error between the motor position and the real joint angle. The result shows that the motor position is above the desired position of 20°, denoted as '3', but the optical joint angle sensor approaches '3' exactly.

Fig. 7(c) displays a torque step response based on impedance control. The experimental result shows the torque step response for seven different steps -10Nmm → -20Nmm → -30Nmm → -40Nmm → -30Nmm → -20Nmm → -10Nmm with 1 second interval. In this experiment, the stiffness K_d=*570 Nmm/rad*, damping B_d=*6000Nmm/rad/s*, and J_d=*0.0*. The overshoots for the loose and tension periods are nearly the same.

Fig. 7(d) shows a typical transition control between free space motion and constrained motion. The desired position denoted as '1' is 21°. The joint moves to this reference position at a speed of 50°/sec until it detects a contact. The control mode is switched automatically from position control to torque control when the contact torque is greater than the threshold value of τ_{th}=*2.5Nmm*. The joint position denoted as '2' does not reach '1' but the torque approaches a desired value with a limited overshooting. It demonstrates the one side of the transition phase: from free space to constrained environment. By following the outputs of dataglove the joint can also move from contact phase to free motion with stability.

7. Conclusions

In this paper a dynamic model of the third joint of DLR's multisensory hand has been established. Sliding mode control has been successfully implemented in the tracking control of the joint in free space. The position error between the motor and active joint during slippage of artificial muscle and tendon transmission is always compensated in real- time to achieve a desired end-point position. A simplified impedance torque control with

desired stiffness, damping, and mass has been also implemented for the contact phase. A parallel observer is used to switch between the two control modes for the transition control from or to contact motion, and the finger behaves like a programmable spring in steady state. The experimental results show the effectiveness of the proposed controller with the essential property of closed-loop system stability. It might serve as a general solution to the problem of impact control in realistic operating environments.

References:

[1] Hirzinger G., J. Butterfaß, S. Knoch, H. Liu, "DLR's Multisensory Articulated Hand", *Int. Symp. On Experimental Robotics, preprints,* pp.28-39, Barcelona, 1997

[2] J. Dietrich, G. Hirzinger, B. Gombert, J. Schott, "On a Unified Concept for a New Generation of Light-Weight-Robots", *Proc. Of the Conf. ISER, Int. Symp. On Experimental Robotics*, June 1989

[3] Hogan N., "Impedance Control: An Approach to Manipulator: Part I-III ", *Trans. ASME J. Dyn. Syst., Meas., Contr.*, Vol. 107, 1985, pp. 1-24.

[4] Volpe R., and P. Khosla, " A Theoretical and Experimental Investigation of Impact Control for Manipulators " *Int. J. Robot. Res.* 12(4), 1993, pp. 351-365.

[5] Utkin V.I., " Variable Structure Systems with Sliding Modes", *IEEE Trans. Automat. Contr.*, vol. AC-22, no. 2, pp. 212-222, 1977.

[6] C. Melchiorri and A. Tonielli, "Sliding Mode Control for a Robotic Hand", *Robotersysteme* 8, pp. 13-20, 1992.

[7] Paul. R, *Robot Manipulators: Mathematics, Programming and Control.* Cambridge, MA: M.I.T Press, 1981.

[8] Mills J.K., Lokhorst D.M., " Control of Robotic Manipulators During Genaral Task Execution: A Discontinuous Control Approach ", *Int. J. Robot. Res.* Vol. 12(2), 1993, pp. 146-163.

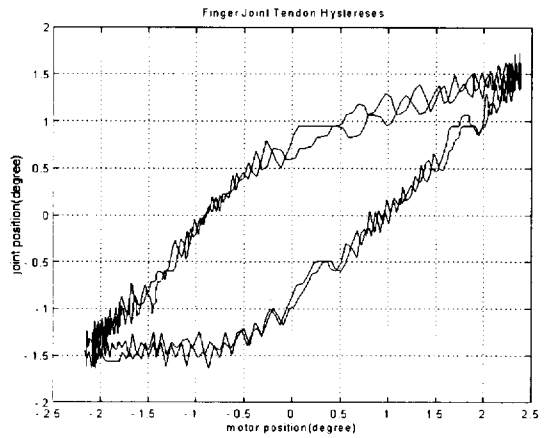

(a)

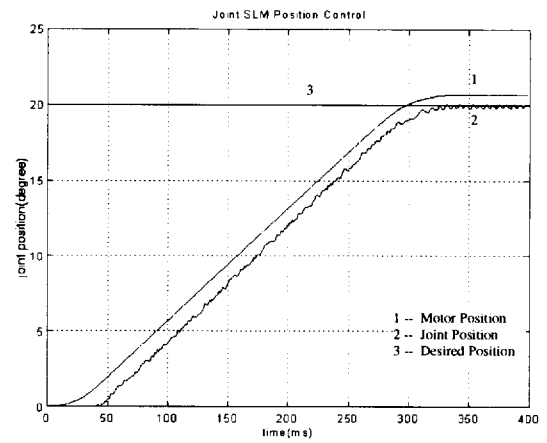

(b)

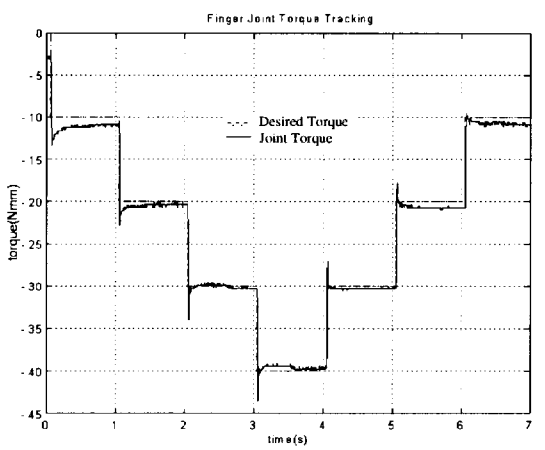

(c)

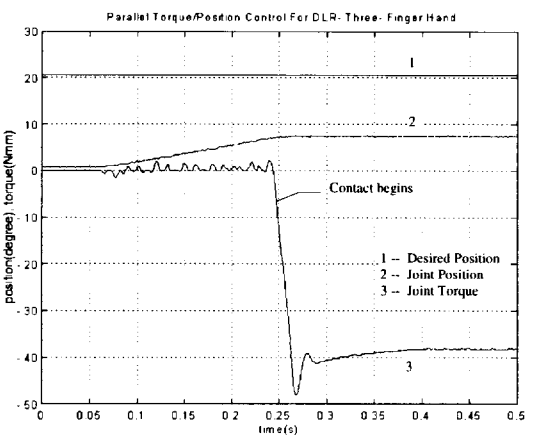

(d)

Fig.7. Some experiments on a finger joint (a) tendon hystereses , (b) joint position control, (c) joint torque tracking, (d) parallel torque/position control